JMEPEG (2024) 33:12742–12752
https://doi.org/10.1007/s11665-023-08845-x

©ASM International
1059-9495/$19.00

ORIGINAL RESEARCH ARTICLE

Preparation and Water Lubrication Behaviors of Al-Cu Alloy-Based Si_3N_4 Composites

Yanan Peng, Chenbo Ma, Qinqwen Dai, Wei Huang, and Xiaolei Wang

Submitted: 3 July 2023 / Revised: 21 August 2023 / Accepted: 29 September 2023 / Published online: 23 October 2023

In this paper, Al-Cu alloy-based Si_3N_4 composite was prepared by using a powder metallurgy technology. The phase, surface appearance and hardness of the composites with different Si_3N_4 contents were investigated. The water lubrication behaviors of Al-Cu alloy-based Si_3N_4 composites were evaluated, and the corresponding low friction mechanisms were explained. Experimental results show that the main structure of sintered Al-Cu alloy contains of α(Al) + θ($CuAl_2$) metal phase. With the addition of Si_3N_4, the AlN, Al_2O_3 and SiAlON ceramic phases appear for the Al-Cu alloy-based Si_3N_4 composites. The composites with 40 wt.% Si_3N_4 content demonstrates flat net structure on the surface with the highest hardness. Under water lubrication condition, the low friction coefficient of 0.05 can only be achieved for the composites with proper Si_3N_4 content. Analysis reveals that the flat contact surface and tribo-chemical reaction seem to be the two essential conditions for the low friction. The major wear mechanisms transfer from mechanically dominated wear at the running-in process to the tribo-chemical dominant at the low friction stage.

Keywords Al-Cu alloy-based Si_3N_4 composites, hardness, low friction, water lubrication

1. Introduction

Oil lubricant is crucial to mechanical equipment, and it may maintain the dominant role in the lubrication area for a long time. However, the environmental pollution is under increasing threat from the overuse of oil, and the presence of the global oil crisis has presented particular challenges for oil lubrication, which makes people seek an alternative urgently since the 1970 s (Ref 1). To resolve the pollution of oil lubrication and save the energy sources, many green lubricants, such as ionic liquids (Ref 2), eco lubricants (Ref 3, 4) and self-organization of the surface layers (Ref 5, 6) have presented a good prospect.

Water is ubiquitous but is often overlooked. It is environmentally friendly, flame retarded, low cost and sustainable as well (Ref 7-12). Adopting water as a lubricant could be an ideal approach to avoid the drawbacks of oil lubrication. Thus, choosing suitable materials as tribo-pairs for water lubrication is of great importance.

Rubber (Ref 13-16) and plastic (Ref 10, 17, 18) were used as water-lubricated materials. It was reported that the groove-shaped rubber bearings have a low friction coefficient of 0.02 under water lubrication condition (Ref 13, 14). However, rubber is prone to elastic deformation, resulting in poor shape retention and low load-bearing capacity. Plastic is a synthetic polymer with the properties of good plasticity, excellent chemical stability and shock absorption. Polytetrafluoroethylene and ultra-high molecular weight polyethylene, as one of the typical representative, have been widely applied in the water lubrication area (Ref 10, 17). The disadvantages of water absorption and poor heat resistance may seriously affect its mechanical properties and dimensional accuracy.

Copper alloys, such as bronze, brass and tin bronze, are also used as water-lubricated materials in the early days (Ref 15, 19, 20). One of the successful application is brass, which is the first water-lubricated material for propeller shafts. These materials possess a high load-bearing capacity, while their weakness is equally notable, such as electrochemical corrosion and poor impact resistance. Recent studies show that ceramic is a suitable candidate for water lubrication (Ref 21-25). It has corrosion resistance, high hardness, high strength, low density and high stiffness. The friction coefficient of self-mated Si_3N_4 and SiC can reach 10^{-3} order of magnitude in water. However, fatal flaws of low fracture toughness and hard machinability limit their applications to a certain extent.

According to available reports, the main properties of the above materials were summarized in terms of corrosion resistance, load-bearing capacity, shape retention, high-temperature stability, wear resistance, impact resistance, machinability and friction coefficient. And the results are shown in Table 1.

Note that copper alloys and ceramics exhibit relatively good performances. It could be a feasible method to preparing metal-based ceramic composite with an excellent water lubrication property. Among the numerous ceramics, Si_3N_4 presents the shorter running-in period in water (Ref 21). When fabricating metal-based Si_3N_4 composite, the interfacial infiltration and wettability between the selected metal and Si_3N_4 is a core problem. Actually, the wettability between Si_3N_4 and several metals, such as Ag, Al, Au, Cu, In and Sn, was studied by Ljungberg et al. (Ref 27), and molten Al shows an outstanding potential, especially at the high temperature of 1100 °C.

Yanan Peng, Qinqwen Dai, Wei Huang, and **Xiaolei Wang**, College of Mechanical and Electrical Engineering, Nanjing University of Aeronautics and Astronautics, Yudao Street 29#, Nanjing 210016, China; and **Chenbo Ma**, School of Mechanical and Electrical Engineering, Nanjing Forestry University, Nanjing 210037, China. Contact e-mail: huangwei@nuaa.edu.cn.

Table 1 Properties of the above-mentioned materials

Properties	Materials			
	Copper (Ref 15, 19, 20)	Rubber (Ref 14-16)	Plastic (Ref 10, 17, 18)	Ceramics (Ref 21-26)
Corrosion resistance	Low	High	Higher	Higher
Load-bearing	High	Low	Low	High
Shape retention	High	Low	Low	Higher
High-temperature stability	≤ 150 °C	≤ 60-70 °C	< 90 °C	≤ 400-500 °C
Wear resistance, mm^3/Nm	10^{-5}	10^{-5}	10^{-5}-10^{-3}	10^{-6}
Machinability method	Turning/Boring/Milling/ Grinding/Planning/Inserting	Grinding/Milling/ Turning/Drilling	Cutting/Punching/Cutting/ Drilling/threading/Laser processing	Ultrasonic/laser Processing/ Diamond grinding/Polishing
Impact resistance	High	High	High	Low
Friction coefficient	0.2-0.3	0.01-0.3	0.04-0.2	≤ 0.01

Recently, research shows that the contact angle between molten Al-10wt.%Cu alloy and Si_3N_4 ceramic is less than 40°, exhibiting good wettability (Ref 28, 29). During the brazing process, it is confirmed that the addition of an appropriate amount of Cu to Al could not only improve the wettability of Al with Si_3N_4 ceramic, but also reduce the sintering temperature (Ref 30, 31).

In this paper, attempts were made to prepare Al-Cu alloy-based Si_3N_4 composite by using the powder metallurgy technology. The influences of the Si_3N_4 content on the phase structure, surface appearance and hardness of the composites were analyzed. Special attention was paid on the water lubrication properties of the Al-Cu alloy-based Si_3N_4 composite.

2. Materials and Methods

2.1 Preparation of Al-Cu Alloy-Based Si_3N_4 Composites

To prepare the Al-Cu alloy-based Si_3N_4 composites, Al-10wt.%Cu alloy powder with the average size of 30 μm was selected as the raw alloy material. And the Si_3N_4 particle with the diameter of 1 μm was used. The Al-Cu alloy-based Si_3N_4 composite wafers were prepared by powder metallurgy. The preparation process was mainly divided into ball milling of dry powders, cold pressing and high-temperature vacuum sintering, as shown in Fig. 1.

The powder of Al-Cu alloy and Si_3N_4 was mixed in a planetary ball milling machine. According to Ref 32-34, the selected ball milling parameters were as follows: the rotation speed of 300 r/min, the ball-to-powder mass ratio of 3:1, and the duration of 8 h with a 10 min pause per hour. After that, the mixed powders were cold pressed into a wafer with the size of $\Phi 15 \times 2$ mm by using an electric powder pressing machine at the pressure of 240 MPa for 5 min. Then, the pressed wafers were placed into a high-temperature vacuum furnace with a vacuum degree of 10-1 Pa for sintering. The sintering parameters are set as follows: temperature rises to 450 °C for 10 min, and then continues to heat up to 1100 °C at the rate of 10 min/°C and holds for 2 h. After that, the sample in the furnace cools to room temperature. The specific sintering process is also given in Fig. 1.

To investigate the effect of Si_3N_4 content on the properties of Al-Cu alloy-based Si_3N_4 composites, the wafers with different components were prepared, as shown in Table 2.

2.2 Characterization of Al-Cu Alloy-Based Si_3N_4 Composites

The phase structure of the sintered wafers was performed by an x-ray diffractometer (D8 Advance A25, Bruker, USA) with Cu $K\alpha$ radiation (λ = 0.15404 nm). The surface appearance of the samples was investigated by a scanning electron microscope (Nova Nano SEM 450, FEI, Japan). The average hardness was obtained by measuring 9 points along the radial direction of the wafer surface via a micro-hardness tester (VMH-002VMA, Lecia, Germany) with the load of 0.2 kgf/cm^2 and loading time of 10 s.

The water lubrication performance of each composite wafer was investigated using a ball-on-disk tribometer and a Si_3N_4 ball with the diameter of 8 mm worked as the counterpart. Figure 2 presents schematic diagram of the test setup. Throughout the test, the contact between the wafer and ball

was completely immersed in the deionized water. The normal load and sliding speed were kept at 2 N and 0.168 m/s, and the total sliding time was 1100 min. To ensure the reliability, each test was carried out 3 times. Due to the component difference, the six wafers present different original roughness. Since the surface quality may affect the friction result, the wafers were polished with the roughness of about 90 $\sim$ 100 nm. The wear scars on the balls and the wear tracks on the wafers were characterized by an optical microscopy, SEM and 3D profilometer (Contour GT-K0, Bruker, USA). Based on the cross-section area of the wear track and the diameter of the wear scar, the wear volumes of the wafer and corresponding ball were calculated.

To further investigate the wear mechanisms, microscopic morphology of the worn surface was characterized by a scanning electron microscope (FE-SEM) equipped with an energy dispersive spectrometer (EDS) (Quanta 200, Philips-FEI, Netherlands). Besides, the wear products dispersed in water were also collected and analyzed with a transmission electron microscope (TEM) (HT7700, Hitachi, Japan).

3. Results and Discussion

3.1 Phase of Al-Cu Alloy-Based Si_3N_4 Composites

The XRD patterns of Al-Cu alloy-based Si_3N_4 composites with varying Si_3N_4 content are shown in Fig. 3. It can be seen that the main structures of wafer A0 are α(Al) + θ($CuAl_2$). With the addition of Si_3N_4 in the composites, AlN, Al_2O_3 and SiAlON ceramic phases, as well as the α(Al) + θ($CuAl_2$) metal phase, form in wafer A1. As mentioned in Ref 35, in a low vacuum environment, Al and O can form amorphous AlO and stable Al_2O_3 through a high-temperature reaction, which may be described in Eq 1 and 2. The formation of AlN can be ascribed to the reaction of Al and Si_3N_4 (see in Eq 3) since the calculated free energy (ΔG) of the reaction is negative. At the same time, the SiAlON is also detected. According to Ref 36, the high temperature may not only accelerate the diffusion of Al in Si_3N_4, but also promote the solution of Al_2O_3 in the Si_3N_4 lattice. Due to the highest content of Si_3N_4 in wafer A5, the more solid solution of Al_2O_3 in Si_3N_4 could be formed. Thus, more SiAlON ceramic phase appears in the wafer A5.

$$Al + O_2 \rightarrow AlO\ (Amorphous) \quad (Eq\ 1)$$

$$Al + O_2 \rightarrow Al_2O_3 \quad (Eq\ 2)$$

$$Si_3N_4 + Al \rightarrow AlN + Si \quad \Delta G < 0 \quad (Eq\ 3)$$

$$Si_3N_4 + AlO \rightarrow SiAlON\ (Sialon) \quad (Eq\ 4)$$

3.2 Surface Appearances of Al-Cu Alloy-Based Si_3N_4 Composites

Figure 4 shows the surface appearances of the six samples after damage-free polishing. As can be seen, the surface of the sample A0 is relatively smooth. With the addition of Si_3N_4, small amount of bright particles appears on the surface of wafer A1. With the increment in the Si_3N_4 content, the microparticles increase gradually (see in Fig. 4, A2).

Obvious difference appears when the Si_3N_4 content exceeds 20wt.%. Compared with wafer A2, a net structure can be found on the surface of A3 wafer, and the bright particles distributed on the surface of wafer A3 decrease sharply. The EDS analysis shows that the elemental compositions of the precipitate are N, O, Al and Si. Combined with the results of the XRD and EDS, it can be deduced that the structure of the bright precipitate could be SiAlON. Compared with the surface appearance of sample A4, more cloddy bulges distribute randomly on the surface of wafer A5. Based on the results of XRD (see in Fig. 3), both the peaks and strengths of SiAlON phase increase

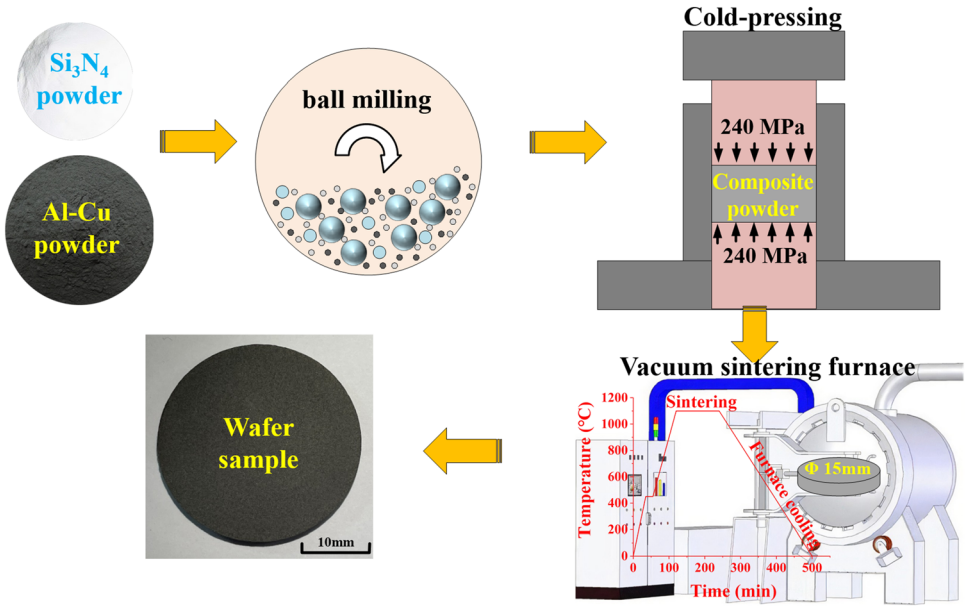

Fig. 1 Preparation process of Al-Cu alloy-based Si_3N_4 composites

Table 2 Al-Cu alloy-based Si_3N_4 composite wafers with different components

Wafer sample	A0	A1	A2	A3	A4	A5
Si_3N_4 mass percent, wt.%	0	10	20	30	40	50

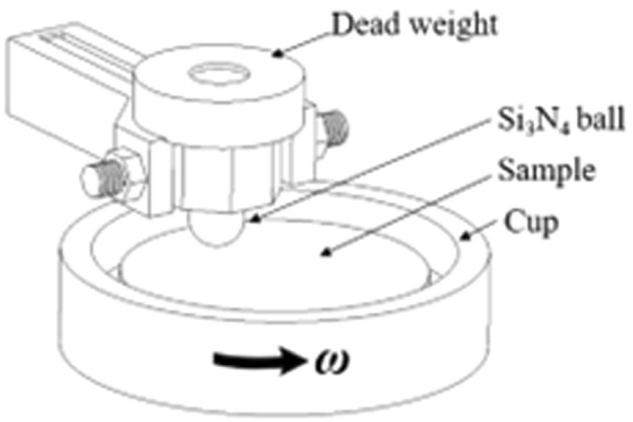

Fig. 2 Schematic diagram of the test setup

for wafer A5. Thus, the cloddy bulges could be SiAlON structure.

3.3 Hardness of Al-Cu Alloy-Based Si_3N_4 Composites

Figure 5 presents the hardness of the six wafers. In order to improve the test accuracy, the wafers were polished to the average roughness of 90-100 nm. The value is the average of 9 points along the radial direction of the wafer surface.

It can be seen that the hardness first increases with the increment in Si_3N_4 content and then decreases. Based on the previous phase structure analysis, the more the Si_3N_4 content is, the more the ceramic phases of AlN, Al_2O_3 and SiAlON form. It is known that the hardness of the three ceramic phases is higher than that of the $\alpha(Al) + \theta(CuAl_2)$ metal phase, which will result in the rise of the hardness. Among the six samples, the maximum value of 628 HV is achieved for A4 wafers. Compared with sample A4, the hardness of A5 decreases to a certain extent. As mentioned above, the high content of the Si_3N_4 may lead to the relative lacking of Al-Cu alloy. In the composite, the Al-Cu alloy plays as a binding phase. Due to the reduction in the binding phase, the compactness of the wafer decreases, which would weaken the surface hardness.

3.4 Water Lubrication Performance of Al-Cu Alloy-Based Si_3N_4 Composites

Figure 6 shows the friction curves of the six samples under water lubrication condition. It can be found that the sample A1 shows the highest coefficient of friction about 0.7 during the whole test process. For the composite samples, there are two kinds of experimental phenomenon. The friction coefficient of samples A1-A4 presents a high value at the very beginning, and it drops gradually with the sliding time. The low and stable friction coefficient of 0.05 can be achieved for each sample after a period of running-in time. Among the four samples, the wafer A4 exhibits the shortest running-in time of 135 min. The only exception is sample A5, and its friction coefficient always stays above 0.2 after sliding in water for 1100 min.

Figure 7 presents the final morphology of the worn surfaces. As can be seen, the wear track on the A0 wafer surface is the widest and deepest. The diameter of the wear scar on the corresponding Si_3N_4 ball is the biggest. And the thick and deep furrows along the sliding direction can also be observed. Many grinding scratches appear on the wear scar of the ball. Combined with the high friction coefficient and severe wear, the abrasive wear could be the dominated mechanism for the tribo-pairs.

Compared with the A0 wafer, the wear tracks on the wafers of A1-A4 become narrow and shallow obviously. Meanwhile, the wear tracks tend to be smoother according to the 3D profile images, which is beneficial to the formation of a better conforming contact interface. What's more, the diameter of the wear scar on the balls decreases gradually. A similar phenomenon for the low friction of self-mated Si_3N_4 was also found by Tomizawa and Fischer (Ref 22), and the wear mechanism could be changed into tribo-chemical wear. While for the sample of A5, the depth of wear track presents a slight increment, and the diameter of the wear scar on the ball also enhances moderately. Compared with sample A0 and samples A1-A4, it seems that the wear mechanism is dominated by mechanical and tribo-chemical wears together. Thus, the sample of A5 maintains a higher friction coefficient during the whole test process.

Based on the cross-section profiles of the wear track (see in Fig. 7) and wear scar on the ball, the wear rate of each tribo-pair is calculated and displayed in Fig. 8, respectively. Not surprisingly, the highest value appears for the A0 wafer with the wear rate of 20.67-24.8 $\times$ 10^{-6} mm^3/m, while for the Al-Cu alloy-based Si_3N_4 composites, the values decrease dramatically and the wear volume of the A4 wafer (with 40 wt.% Si_3N_4 content) is the lowest with the value of about 0.58-2.07 $\times$ 10^{-6} mm^3/m, which is reduced by a factor of 10 compared with that of A0 sample. Again, wear volume of A5 wafer increases in a certain degree. Even so, the value is still lower than that of A0 sample. Due to the formation of AlN, Al_2O_3 and SiAlON in Al-Cu alloy-based Si_3N_4 composites, the increased hardness of the wafers may help to improve the wear resistance and decrease the wear volume as well.

Overall, wear volume of the Si_3N_4 balls present the similar variation tendency as the wafers. The ball sliding with the A0 wafer presents the highest wear volume, which is result from the pure mechanical wear. On the contrary, the reduced wear volume of the balls may be ascribed to the tribo-chemical reaction of Si_3N_4 ball in water (Ref 37-39), which will be explained in more detail in the next section.

To further figure out the mechanism of the low friction and wear, the worn surfaces (A4 wafers and Si_3N_4 ball) were observed at the two typical friction stages. As shown in Fig. 6, the evolution of friction curve of A4 wafer can be divided into a running-in period and a stable friction period. The width of the wear track is about 560 μm after the first 135 min of running-in time (see in Fig. 9), and the value increases to 702 μm at the end of the test (1100 min). The wear volumes of the wafer and ball are about 0.014 and 0.006 mm^3 after the running-in time. Although another more 965 min sliding was carried out, only a slight increase in the wear volumes (0.004 and 0.006 mm^3) appears for the wafer and the ball. It seems that the major wear mechanism could be mechanical wear at the high friction

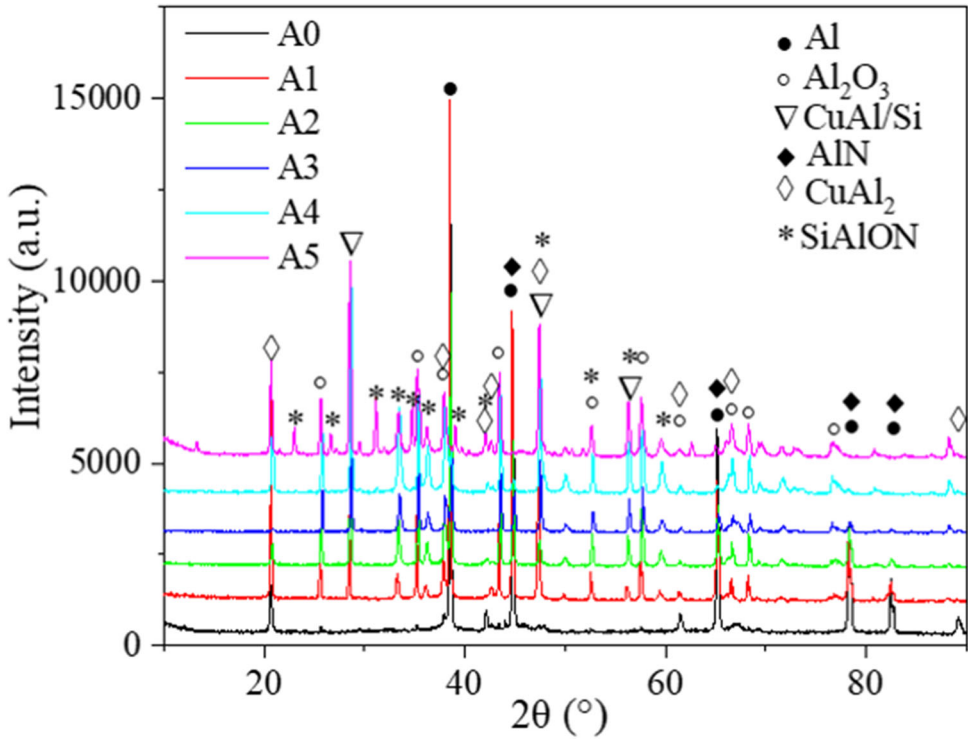

Fig. 3 XRD patterns of the six wafers

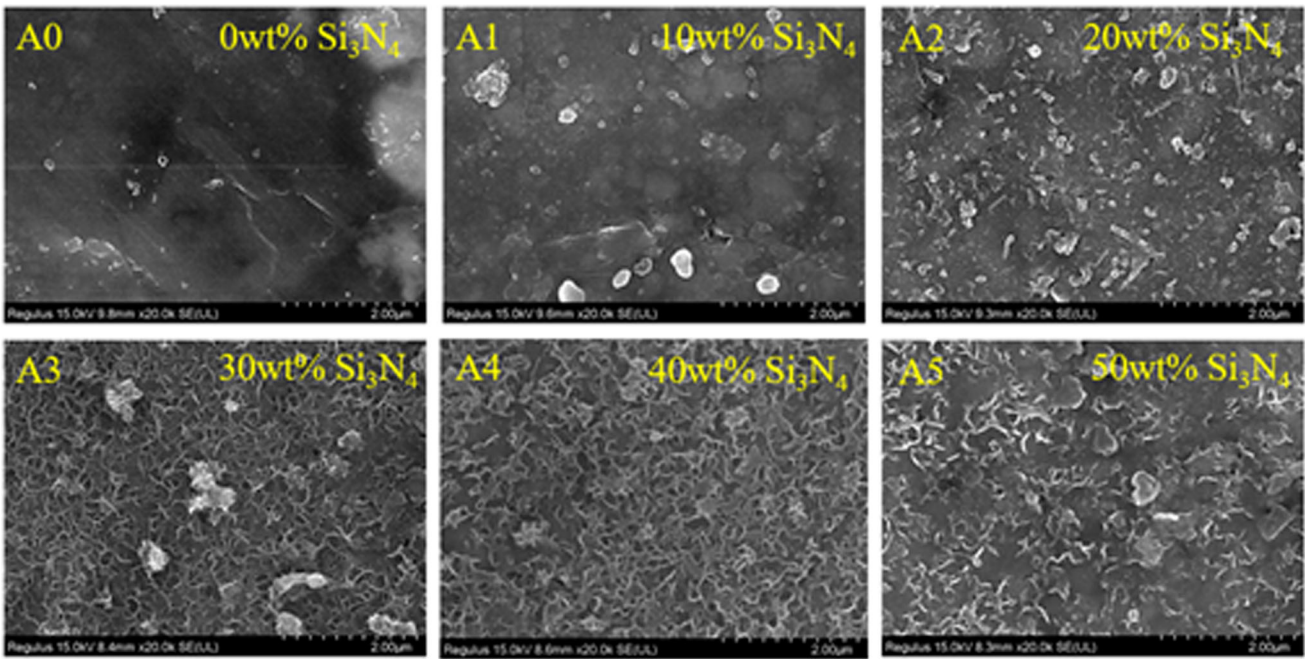

Fig. 4 Surface appearance of the six wafers

process and it transits to tribo-chemical wear dominated at the lower and stable frictional stage.

More detailed information on the worn track is shown in Fig. 10. Compared with the initial surface, not only the matrix, but also the network structures are grinded. The worn surface of the track is quite flat and it looks like a polished one after sliding in water for 1100 min. Based on the images of the worn surface, it can be speculated that the continuous and flat contact surface might be one of the essential conditions for the low friction.

Besides, the EDS analysis indicates that the main element in the flat track contains N, O, Al, Si and a small amount of Cu. As mentioned in Ref 37, 38, 40-43, hydrated silica can be formed as a product of the tribo-chemical reaction between Si_3N_4 and water ($\Delta G = -566.5$ kJ/mol for the formation of SiO_2). Meanwhile, alumina can also react with water to form

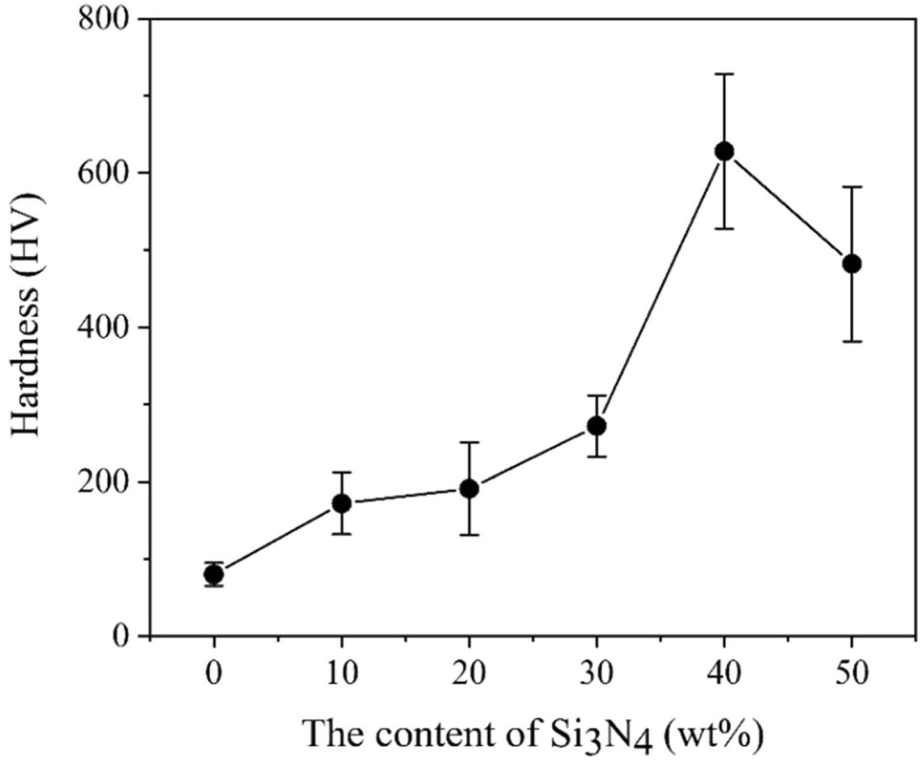

Fig. 5 Hardness of the of the six wafers

aluminum hydroxides during the friction process according to the free energy calculation ($\Delta G = -21.6$ kJ/mol for the formation of aluminum hydroxide) (Ref 44). Since the free energy of these two tribo-chemical reactions is negative, it is quite likely that the lower friction is related to the formation of silicon hydroxide and aluminum hydroxide, which may play as good boundary lubrication film to increase the bearing capacity (Ref 22, 37, 41) and to decrease the shear stress. In addition, the result of molecular dynamics simulations also shows that the hydrolysis reaction of the Si-based ceramic can be mechanically induced at the sliding interface by friction (Ref 45), and double tribo-layers consisting of a colloidal silica layer and a hydrophilic hydrate are self-formed at the sliding interface (Ref 46). Thus, the low friction coefficient appears, and the wear volume keeps a little increase in the stable friction stage.

To figure out the tribo-chemical reactions, morphologies and chemical composition of the wear products formed in the lubricant were detected. As shown in Fig. 11, the lubricant collected after 1100 min friction test presents milk white compared with the deionized water, which indirectly confirms the tribo-chemical reactions. The lamellar structured wear debris with the size of 30-40 nanometers can be observed from the TEM image. Due to the size effect, serious aggregation occurs. The electron diffraction pattern indicates that these particles are mainly polycrystalline phase. According to the EDS, elements N, O, Al, Si and Cu are detected, which may also reflect the formation of silicon hydroxide and aluminum hydroxide. Therefore, besides the smooth worn surface, the hydration products could be the other reason for the low friction. The corresponding wear mode may change from the mechanical to tribo-chemical wear in the low friction stage.

4. Conclusions

In this paper, a kind of water-lubricated material, Al-Cu alloy-based Si_3N_4 composite was successfully fabricated by using powder metallurgy technology. The effect of Si_3N_4 content on the phase structure, surface appearance and hardness was studied. Much attention was paid on the water lubrication properties of the composite.

Owing to the excellent wettability of Al with Si_3N_4 ceramics, the Al-Cu alloy-based Si_3N_4 composites can be prepared by vacuum sintering at 1100 °C. The phase of sintering Al-Cu alloy (A0 wafer) mainly contains α-Al and θ-$CuAl_2$. With the addition of Si_3N_4 in the composites, metal phases of the α-Al and θ-$CuAl_2$ are gradually transformed into AlN, Al_2O_3 and SiAlON ceramic. Meanwhile, the surface appearance also changes with the variation of Si_3N_4 content. The precipitate distributed on the surface decreases with the increase in Si_3N_4 content and flat network structure forms for the wafer A4 with the 40wt.% Si_3N_4 content. The appropriate amount of Si_3N_4 plays the strengthen effect, and the composite with 40wt.% Si_3N_4 content presents the highest hardness of 628 HV. Water lubrication property of the composite is also related with the Si_3N_4 content, and low friction coefficient only appears for samples A1-A4. To achieve low friction, the flat wear track and tribo-chemical reaction seem to be the two essential conditions. During the total friction course, the major wear mechanisms transfer from mechanically dominated wear at the running-in process to the tribo-chemical dominant at the low friction stage.

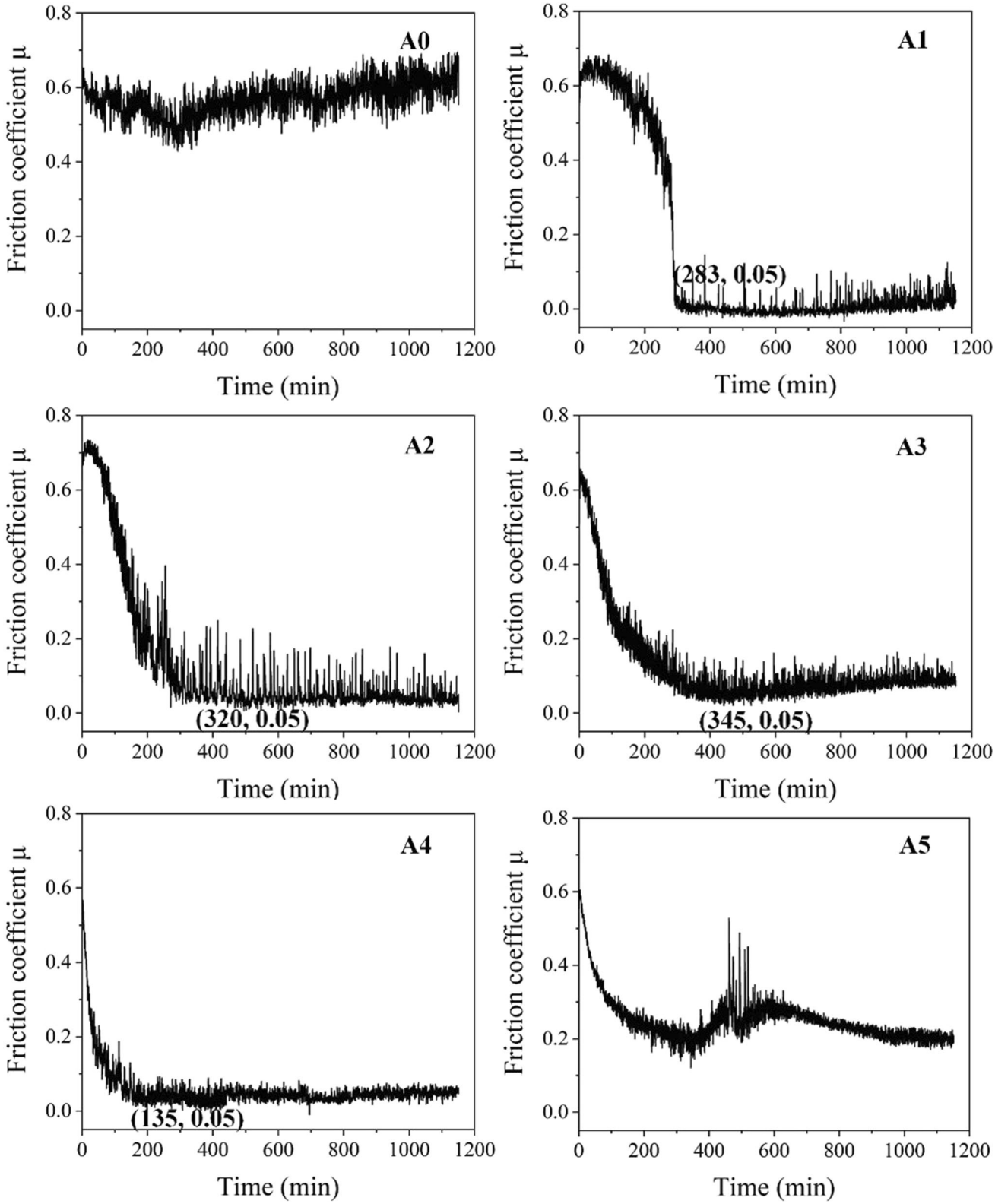

Fig. 6 Friction curves of the six samples sliding in water

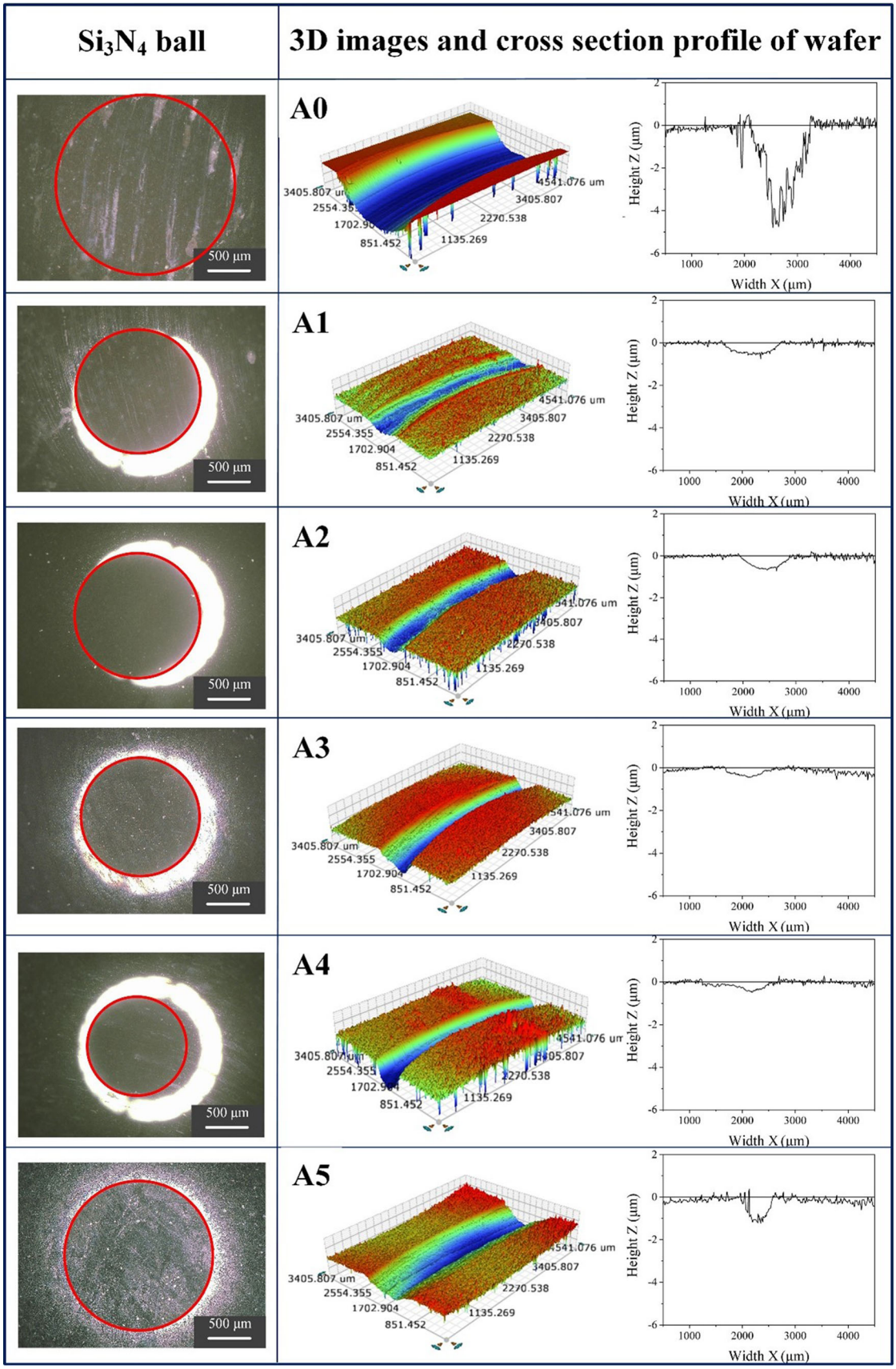

Fig. 7 Wear morphologies of the Si_3N_4 balls and wafers

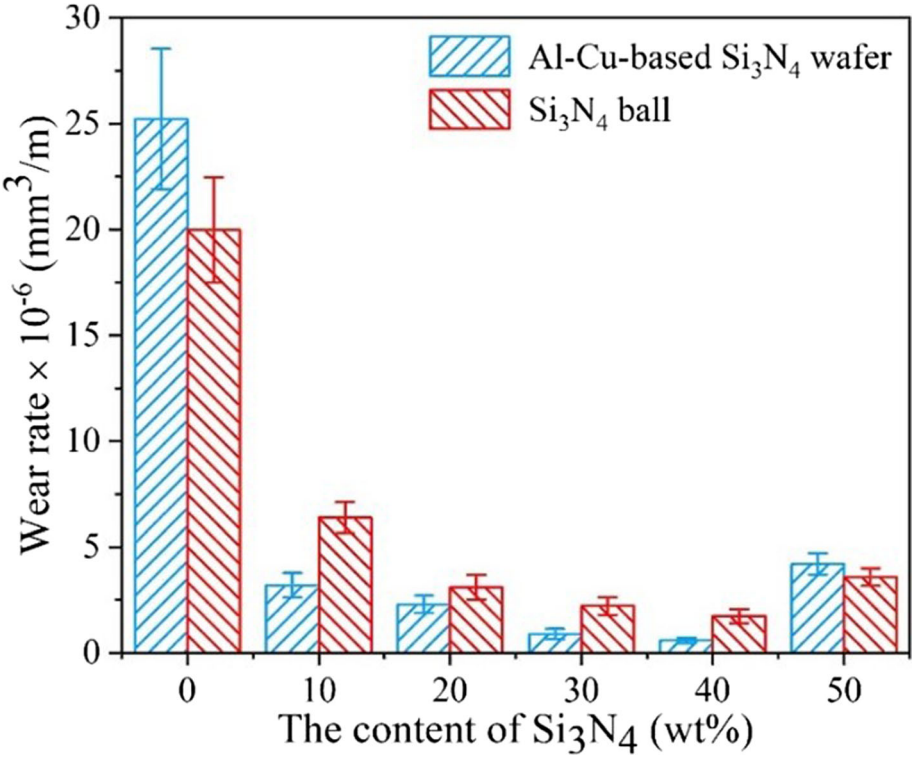

Fig. 8 Wear rate of the wafers and the Si_3N_4 balls

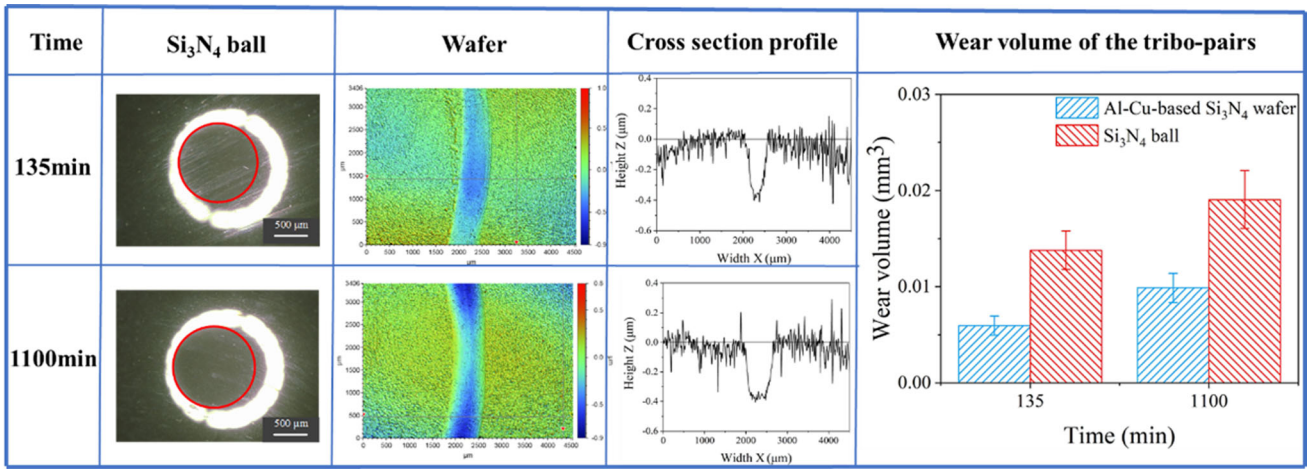

Fig. 9 Worn surfaces and wear volumes of Si_3N_4 ball and A4 wafer at two stages

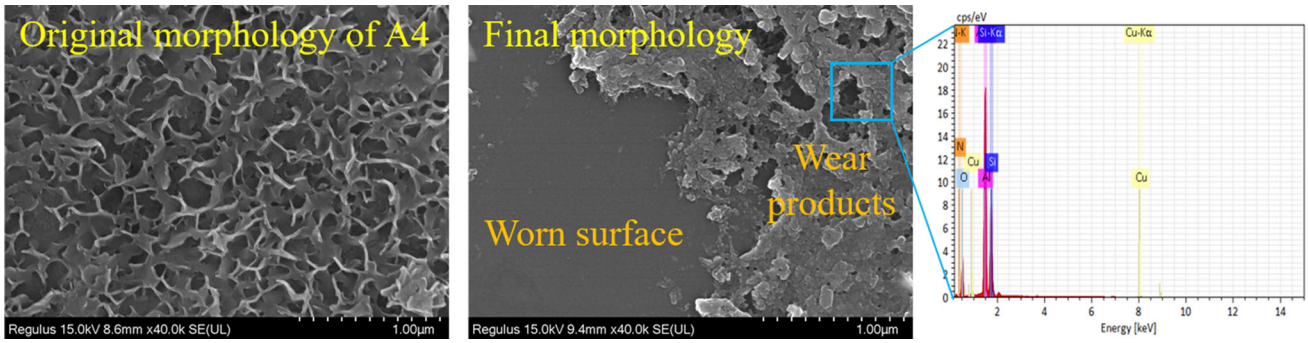

Fig. 10 Morphology comparison of the A4 wafer before and after the friction test

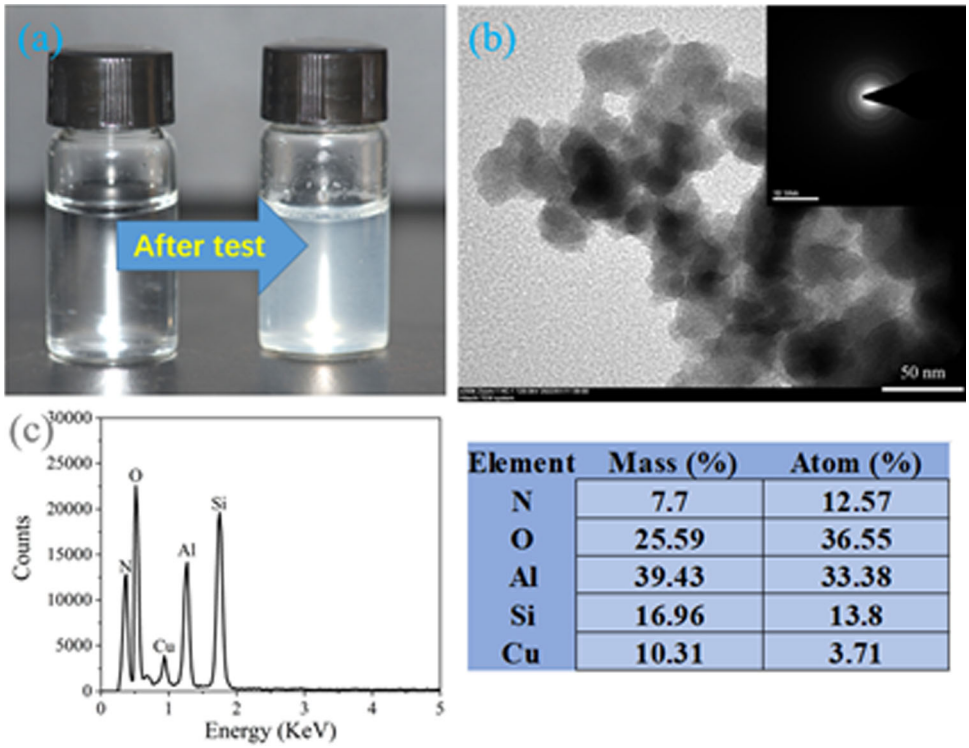

Element	Mass (%)	Atom (%)
N	7.7	12.57
O	25.59	36.55
Al	39.43	33.38
Si	16.96	13.8
Cu	10.31	3.71

Fig. 11 (a) Water before and after test, (b) TEM image and EDS of the wear products suspended in the water and (c) EDS of the wear products

Acknowledgment

The authors thank the National Key Laboratory of Science and Technology on Helicopter Transmission (Grant No. HTL-A-22G14).

Author Contribution

Conceptualization was done by XW; investigation was done by YP and CM; writing—original draft was done by YP; writing—review and editing was done by WH and QD; funding acquisition was done by WH. All authors have read and agreed to the published version of the manuscript.

Conflict of interest

The authors declare that they have no conflict of interest.

References

1. Q. Wang and F. Zhou, Progress in Tribological Properties of Nano-Composite Hard Coatings under Water Lubrication, *Lubricants*, 2017, **5**(1), p 5
2. M. Michalec, P. Svoboda, I. Krupka, M. Hartl, and A. Vencl, Investigation of the Tribological Performance of Ionic Liquids in Non-conformal EHL Contacts under Electric Field Activation, *Friction*, 2020, **8**(5), p 982–994
3. T. Babu and M. Akter, Areas of Green Tribology: A Review, *Tribol. Mater.*, 2023, **2**(1), p 38–45
4. M. Kandeva, Z. Kalitchin, E. Zadorozhnaya, and A. Vencl, Performance Characteristics of Lubricant Based on Rapeseed Oil Containing Different Amounts of Metal-Containing Additive, *Ind. Lubr. Tribol.*, 2022, **3**(74), p 309–315
5. A. Vanossi, C. Bechinger, and M. Urbakh, Structural Lubricity in Soft and Hard Matter Systems, *Nat. Commun.*, 2020, **11**(1), p 4657
6. E. Assenova and A. Vencl, Tribology and Self-Organization in Reducing Friction: A Brief Review, *Tribol. Mater.*, 2022, **1**(1), p 35–41
7. R. Mallya, S.B. Shenoy, and R. Pai, Steady State Characteristics of Misaligned Multiple Axial Groove Water-Lubricated Journal Bearing, *Proc. Inst. Mech. Eng. Part J J. Eng.*, 2014, **229**(6), p 712–722
8. X. Wang, K. Kato, K. Adachi, and K. Aizawa, Loads Carrying Capacity Map for the Surface Texture Design of SiC Thrust Bearing Sliding in Water, *Tribol. Int.*, 2003, **36**(3), p 189–197
9. G. Zhang, Y. Liu, F. Guo, X. Liu, and Y. Wang, Friction Characteristics of Impregnated and Non-impregnated Graphite Against Cemented Carbide under Water Lubrication, *J. Mater. Sci. Technol.*, 2017, **33**(10), p 1203–1209
10. J. Wang, B. Chen, N. Liu, G. Han, and F. Yan, Combined Effects of Fiber/Matrix Interface and Water Absorption on the Tribological Behaviors of Water-Lubricated Polytetrafluoroethylene-Based Composites Reinforced with Carbon and Basalt Fibers, *Compos. Part A Appl. Sci.*, 2014, **59**, p 85–92
11. J.H. Ri and R.G. Ripeanu, Evaluation of the Wear and Corrosion Resistance of Coated Parallel Gate Valve, *Tribol. Mater.*, 2022, **1**(1), p 11–20
12. M. Kandeva, M. Zagorski, R. Nikolić, B. Stojanović, A. But, and F. Botko et al., Friction Properties of the Heat-Treated Electroless Ni Coatings Embedded with c-BN Nanoparticles, *Coatings*, 2022, **12**(7), p 1008
13. W.F. Busse and W.H. Denton, Water-Lubricated Soft-Rubber Bearings, *Trans. ASME*, 1932, **54**, p 3–10
14. A. Fogg and S.A. Hunwicks, Some Experiments with Water-Lubricated Rubber Bearings, *Gen. Discuss. Lubr. Lubr.*, 1937, **1**, p 101–106
15. R. Orndorff, Water-Lubricated Rubber Bearings, History and New Developments, *Nav. Eng. J.*, 1985, **97**(7), p 39–52
16. B. Bhushan, S. Gray, and R.W. Graham, Development of Low-Friction Elastomers for Bearings and Seals, *Lubr. Eng.*, 1982, **38**, p 626–634
17. G.Y. Xie, G.X. Sui, and R. Yang, Effects of Potassium Titanate Whiskers and Carbon Fibers on the Wear Behavior of Polyetheretherketone Composite under Water Lubricated Condition, *Compos. Sci. Technol.*, 2011, **71**(6), p 828–835

18. T.L. Daugherty and N.T. Sides, Frictional Characteristics of Water-Lubricated Compliant-Surface Stave Bearings, *ASLE Trans.*, 1981, **24**(3), p 293–301
19. N.M. Franchek, D.W. Childs, and L.S. Andres, Theoretical and Experimental Comparisons for Rotordynamic Coefficients of a High-Speed, High-Pressure, Orifice-Compensated Hybrid Bearing, *J. Tribol. Trans. Asme*, 1995, **117**(2), p 285–290
20. J.K. Lancaster, A Review of the Influence of Environmental Humidity and Water on Friction, Lubrication and Wear, *Tribol. Int.*, 1990, **23**(6), p 371–389
21. T.E. Fischer and H. Tomizawa, Interaction of Tribochemistry and Microfracture in the Friction and Wear of Silicon Nitride, *Wear*, 1985, **105**(1), p 29–45
22. H. Tomizawa and T.E. Fischer, Friction and Wear of Silicon Nitride and Silicon Carbide in Water: Hydrodynamic Lubrication at Low Sliding Speed Obtained by Tribochemical Wear, *ASLE Trans.*, 1987, **30**(1), p 41–46
23. S. Jahanmir and T.E. Fischer, Friction and Wear of Silicon Nitride Lubricated by Humid Air, Water, Hexadecane and Hexadecane + 0.5 percent Stearic Acid, *Tribol. Trans.*, 1988, **31**(1), p 32–43
24. J.K. Lancaster, Y. Mashal, and A.G. Atkins, The Role of Water in the Wear of Ceramics, *J. Phys. D Appl. Phys.*, 1992, **25**(1A), p A205–A211
25. B. Löffelbein, M. Woydt, and K.H. Habig, Sliding Friction and Wear of Ceramics in Neutral, Acid and Basic Aqueous Solutions, *Wear*, 1993, **162–164**, p 220–228
26. P. Andersson and P. Lintula, Load-Carrying Capability of Water-Lubricated Ceramic Journal Bearings, *Tribol. Int.*, 1994, **27**(5), p 315–321
27. L. Ljungberg and R. Warren, Wetting of Silicon Nitride with Selected Metals and Alloys, *Ceram. Eng. Sci. Proc.*, 1989, **10**(11), p 1655–1666
28. M. Naka, M. Kubo, and I. Okamoto, Wettability of Silicon Nitride by Aluminium, Copper and Silver, *J. Mater. Sci. Lett.*, 1987, **6**(8), p 965–966
29. M. Naka, M. Kubo, and I. Okamoto, Brazing of Si_3N_4 to Metals with Al-Cu Filler Metals(Physics, Process, Instrument & Measurement), *Trans. JWRI*, 1990, **19**(1), p 33–38
30. M. Naka, Controlling of Ceramic-Metal Interfacial Structure Using Molten Metals, *Trans. JWRI*, 1992, **21**(1), p 1–07
31. D.S. Han, H. Jones, and H.V. Atkinson, The Wettability of Silicon Carbide by Liquid Aluminium: The Effect of Free Silicon in the Carbide and of Magnesium, Silicon and Copper Alloy Additions to the Aluminium, *J. Mater. Sci.*, 1993, **28**(10), p 2654–2658
32. M. Shojaei, A. Hasani, Z. Amiri, and G.R. Khayati, Using the Group Method for the Synthesis of Copper/ZrO_2 Nanocomposites to Achieve High Wear Resistance by Ball Milling and Spark Plasma Sintering, *Ceram. Int.*, 2022, **48**(12), p 17576–17588
33. J. Christudasjustus, C.S. Witharamage, G. Walunj, T. Borkar, and R.K. Gupta, The Influence of Spark Plasma Sintering Temperatures on the Microstructure, Hardness, and Elastic Modulus of the Nanocrystalline $Al_{-x}V$ Alloys Produced by High-Energy Ball Milling, *J. Mater. Sci. Technol.*, 2022, **122**, p 68–76
34. J. Huang, Y. Zhang, D. Wang, B. Ren, P. Song, and G. Zhang et al., Effect of Ball Milling Process on the Mechanical and Thermal Properties of the Nanodiamond/2024Al Composites, *Micron*, 2021, **148**, p 103104
35. X.S. Ning, K. Suganuma, M. Morita, and T. Okamoto, Interfacial Reaction Between Silicon Nitride and Aluminium, *Philos. Mag. Lett.*, 1987, **55**(3), p 93–97
36. X.S. Ning, T. Okamoto, Y. Miyamoto, A. Koreeda, and K. Suganuma, Reaction Chemistry at Joined Interfaces Between Silicon Nitride and Aluminium, *J. Mater. Sci.*, 1991, **26**(15), p 4142–4149
37. M. Chen, K. Kato, and K. Adachi, Friction and Wear of Self-Mated SiC and Si_3N_4 Sliding in Water, *Wear*, 2001, **250**(1), p 246–255
38. V. Ferreira, H.N. Yoshimura, and A. Sinatora, Ultra-low Friction Coefficient in Alumina–Silicon Nitride Pair Lubricated with Water, *Wear*, 2012, **296**(1–2), p 656–659
39. H. Yamakiri, S. Sasaki, T. Kurita, and N. Kasashima, Effects of Laser Surface Texturing on Friction Behavior of Silicon Nitride under Lubrication with Water, *Tribol. Int.*, 2011, **44**(5), p 579–584
40. M. Chen, K. Kato, and K. Adachi, The Difference in Running-In Period and Friction Coefficient Between Self-Mated Si_3N_4 and SiC under Water Lubrication, *Tribol. Lett.*, 2001, **11**(1), p 23–28
41. J. Xu and K. Kato, Formation of Tribochemical Layer of Ceramics Sliding in Water and its Role for Low Friction, *Wear*, 2000, **245**(1), p 61–75
42. F. Zhou, X. Wang, K. Adachi, and K. Kato, Influence of Normal Load and Sliding Speed on the Tribological Property of Amorphous Carbon Nitride Coatings Sliding Against Si_3N_4 Balls in Water, *Surf. Coat. Technol.*, 2008, **202**(15), p 3519–3528
43. J. Xu, K. Kato, and T. Hirayama, The Transition of Wear Mode during the Running-in Process of Silicon Nitride Sliding in Water, *Wear*, 1997, **205**(1), p 55–63
44. D. Amutha Rani, Y. Yoshizawa, H. Hyuga, K. Hirao, and Y. Yamauchi, Tribological Behavior of Ceramic Materials (Si_3N_4, SiC and Al_2O_3) in Aqueous Medium, *J. Eur. Ceram. Soc.*, 2004, **24**(10–11), p 3279–3284
45. Y. Ootani, J. Xu, T. Hatano, and M. Kubo, Contrasting Roles of Water at Sliding Interfaces Between Silicon-Based Materials: First-Principles Molecular Dynamics Sliding Simulations, *J. Phys. Chem. C*, 2018, **122**(19), p 10459–10467
46. Y. Ootani, J. Xu, N. Takahashi, K. Akagami, S. Sakaki, and Y. Wang et al., Self-Formed Double Tribolayers Play Collaborative Roles in Achieving Superlow Friction in an Aqueous Environment, *J. Phys. Chem. C*, 2020, **124**(15), p 8295–8303

Publisher's Note Springer Nature remains neutral with regard to jurisdictional claims in published maps and institutional affiliations.

Springer Nature or its licensor (e.g. a society or other partner) holds exclusive rights to this article under a publishing agreement with the author(s) or other rightsholder(s); author self-archiving of the accepted manuscript version of this article is solely governed by the terms of such publishing agreement and applicable law.